ELSEVIER

Brain & Development 1996; **18**: 379–388

Original article

Regional MRI measurements of the corpus callosum: a methodological and developmental study

Jagath C. Rajapakse [a,*], Jay N. Giedd [a], Judith M. Rumsey [a], A. Catherine Vaituzis [a], Susan D. Hamburger [a], Judith L. Rapoport [a]

[a] *Child Psychiatry Branch, National Institute of Mental Health, National Institutes of Health, Building 10, Room 6N240, 10 Center Drive, MSC 1600, Bethesda, MD 20892-1600, USA*

Received 6 November 1995; accepted 28 February 1996

A technique for quantifying the midsagittal size and shape of the corpus callosum (CC) from magnetic resonance brain scans is presented. The technique utilizes the distances to the ventral and dorsal boundaries of small sectors of the CC from a reference point to compute the size and shape parameters of the CC and its subdivisions. Intrarater and interrater interclass correlation coefficients for the area measurements ranged from 0.88 to 0.99. Correlations between these automated measures and those obtained by pixel counting were equally high. The corpus callosa of 104 (57 male and 47 female) right-handed healthy children and adolescents, ages 4–18, were examined in relation to age and sex. Corpus callosum growth was most striking for the splenium and isthmus with some changes in the midbody regions. The area and perimeter of these regions increased, shapes became more compact, and the boundaries became more regular with age. The length and curvature at the anterior and posterior regions of the CC increased more rapidly in males than in females. These significant and consistent results indicate that the method is reliable and sensitive to developmental changes of the CC.

Keywords: Corpus callosum; Magnetic resonance imaging; Brain imaging; Interhemispheric communication; Shape measurement

1. INTRODUCTION

The corpus callosum (CC) is the largest interhemispheric commissure in the human brain. It consists of approximately 200 million interhemispheric fibers [1,2], most of which connect homologous regions of the cerebral cortex [3,4]. Although each hemisphere can perceive, think and emote separately and simultaneously [5,6], interhemispheric connections are crucial for many forms of unified motor, sensory and cognitive performance [7–9]. As the interhemispheric fibers generally connect homologous cortical regions via the shortest route, the CC maintains a roughly homotopic pattern with fibers connecting frontal and motor regions traversing through anterior sections and those connecting parietal and occipital regions traversing through the posterior sections.

Corpus callosum morphology has been studied in relation to gender [10–24], psychiatric diagnosis [25–42], age [14–16,43–48], handedness [9,10,22,23,49,50] and brain symmetry patterns [11,13,51,52]. Although there is preliminary evidence that the CC may carry a different number of fibers in males and females and in dextrals as opposed to sinistrals, controversies exist among the findings related to CC shape and size. The inconsistency of the findings may be related to methodological differences, different sample sizes, difficulty in quantifying the complex shape of the CC, and individual variability of the CC morphology. For these reasons, methodological issues and sample characteristics play an important role in the examination of CC morphology.

Magnetic resonance (MR) imaging provides the most resolute images of the CC compared with the other imaging modalities [53]. The CC is clearly delineated on the midsagittal plane of MR brain images and can be outlined manually or using a simple thresholding technique. There are no anatomical landmarks in the midsagittal view of the CC to define corresponding areas of the cortex from which the fibers originate. Attempts to subdivide the CC are often based on the length of a line connecting its most anterior (ACC) and posterior (PCC) points. A scheme of regional divisions depicting the origins of the fibers through the CC, proposed by Witelson [10], is shown in Fig. 1. Another scheme

* Corresponding author. Fax: (1) (301) 402-0296; e-mail: jcr@helix.nih.gov

PII S0387-7604(96)00034-4

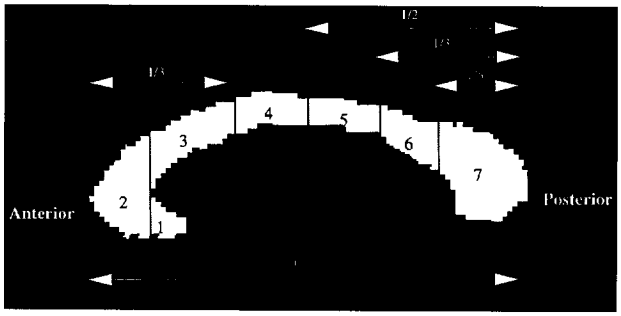

Fig. 1. Regional subdivisions of the corpus callosum, adapted from Witelson et al. (1989). Subregions : (1) rostrum, (2) genu, (3) rostral body, (4) anterior midbody, (5) posterior midbody, (6) isthmus, (7) splenium.

based on five equal divisions of ACC-PCC length and radial lines from the midpoint of ACC-PCC line [30,51] is shown in Fig. 2. A major drawback of the latter division scheme, however, is its inability to demarcate the anterior part of the CC as the rostrum, genu and rostral body. A statistical scheme of regional subdivisions was recently proposed using factor analysis of the CC percentile widths [16,54–56], but the question remains open as to whether the mathematical solution is isomorphic with anatomical projections.

Fourier analysis [57–59], hidden Markov models [60], and calculation of moments [61] have been proposed for analysis, quantification and comparison of closed shapes. But when the shape is complex, the number of harmonics or coefficients representing the shape in these methods become large and differences become minute. Therefore, the above techniques have not been used for the shape analysis of the CC except for one study where a Fourier technique was applied to analyze the most anterior and posterior regions of the CC [62]. In quantifying CC morphology, a representation generating a number of parameters related to different aspects of its shape seems more practical. To characterize the shape of the CC, its length, width, and height [16,47,55] and some specific angles subtended on fixed anatomical landmarks [28,42] have been measured. These measurements render global information on CC but do not provide region specific variations in CC morphology. Because of the heterogeneous nature of the CC, a technique to quantify the size and shape of different regions may be useful in identifying subtle differences in CC morphology among different individuals.

Clinical researchers have been interested in investigating the shape of the CC since early reports of developmental changes, and sexual dimorphism in the shape of the splenium [15,18]. A recent study found more slender corpus callosa in female than in male [24]. Moreover, different callosal shapes have been observed for various neuropsychiatric disorders [29,42,47,62]. Fourier analysis suggested different shapes between normal and schizophrenic cotwins in the second harmonic of the anterior and middle segments of the CC [62]. A significant increase in mean callosal thickness was found in middle and anterior parts of the CC in schizophrenics [29].

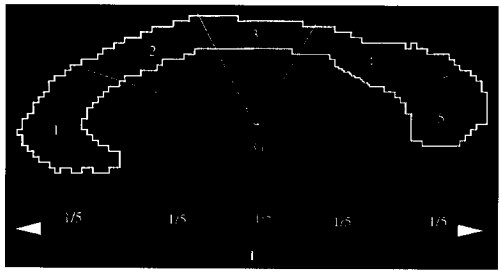

Fig. 2. Illustration of five regional subdivisions of the corpus callosum based on equal divisions of ACC-PCC line and radial lines from a reference point G.

The purpose of this report is to present an automated technique to quantify both the size and shape of the CC and its subdivisions. Witelson's scheme of subdivisions was chosen because the divisions have been used for human CC studies involving a priori hypotheses linking certain segments to particular cortical regions. In addition to quantifying size, the present technique calculates eight parameters related to shape. This report describes the methodology, defines the shape parameters, and relates the technique to other existing methods.

A second objective of this paper is the application of this method to MR brain scans from a large pediatric sample collected in our laboratory. This technique has already been applied to a subset of this population to measure the regional areas and posterior regional CC growth from 4 to 18 years [48]. The present report extends the study to examine shape parameters with respect to age and sex since regional shape measurements of the CC have not earlier been considered in any development study. Because our normative sample did not have enough non-right-handed subjects for meaningful statistical analysis, only right-handed subjects were included in the study.

2. SUBJECTS AND METHODS

2.1. Subject selection

Healthy children and adolescents from ages 4 to 18 were recruited from the community. The details of subject screening which included physical and neurological examination, psychological testing, and medical and psychiatric history are presented elsewhere [63]. One hundred four (57 male and 47 female) right-handed healthy subjects were selected for this study. The scans of all subjects were read as normal by a clinical neuroradiologist at the NIH Clinical Center. Handedness of subjects was determined by the 12 handedness items from Physical and Neurological Examination for Subtle Signs (PANESS) inventory [64]. Subjects indicating a right-hand dominance on 11 or more out of 12 items were designated as right-handed.

2.2. Image acquisition

All subjects were scanned on a General Electric 1.5 Tesla MR imaging scanner. A 3-D spoiled gradient recalled echo sequence in the steady state (3D SPGR) was used (TE = 5 ms, TR = 25 ms, flip angle = 45°, acquisition matrix = 192 × 256, number of repetitions = 1, field of view = 24 cm) to generate 124 1.5-mm thick contiguous axial slices.

2.3. Image processing

The 16-bit images were converted to 8-bit images to facilitate computer processing and transferred to a Macintosh computer workstation to be analyzed with NIH Image [65]. A midsagittal plane image was generated from 3-D axial data set by drawing a

line on a selected axial slice to bisect the cerebral hemispheres and reconstructed using the Reslice function in NIH Image. The midsagittal plane was magnified nine times and verified by the patency of the cerebral aqueduct, the presence of the septum pellucidum and a distinct thalamus. A local elliptical region enclosing the CC was thresholded in an operator supervised manner to isolate the structure. Ventral areas where thresholded structure came in contact with the fornix or septum pellucidum were manually edited to extract the CC. The $X-Y$ coordinates of the CC boundary were saved and transferred to a Unix workstation for the use with the shape program. Total cerebral volume was also determined from 3-D axial data set using a previously described method [63].

2.4. Shape and size measurements

Before regional measurements were determined, ACC and PCC points of the CC were estimated and the outline was rotated until ACC-PCC line became horizontal. This was done iteratively while verifying the ACC and PCC points with each new orientation of the CC. The midpoint G of the ACC-PCC line was considered as the reference point for the rest of the analysis (see Fig. 3). The angle subtended by the CC on G was divided into N equal angles by $N+1$ radial lines drawn from G partitioning the CC into N regional sectors. A sector represents a region of CC delimited by two adjacent radial lines.

The average distances to the ventral and dorsal boundaries of the sectors from the reference point were measured. A representative sector PQSR in region **R** is shown in Fig. 4 where r_1 and r_2 are the average distances from G to the ventral and dorsal boundaries of the sector, respectively. The following set of summations $\{S_1, S_2, S_3\}$ of distances were computed over all the sectors in the region **R** in order to measure the area and shape parameters:

$$S_2 = \sum_R r_1$$

$$S_2 = \sum_R r_2$$

$$S_3 = \sum_R (r_2 - r_1)(r_2 - r_1)$$

With the above summations, the following parameters were computed for every regional subdivision of the CC: (1) area: midsagittal surface area of the region; (2) perimeter: total length along the boundary of the region; (3) compactness: ratio of the area to the perimeter of the region; (4) distance to the center of gravity (CG): distance from the reference point G to the center of the gravity of the region; (5) width: average length of the distances between corresponding dorsal and ventral boundary points of sectors that comprise the region; (6) maximum width: maximum length of the lines connecting the corresponding dorsal and ventral points of the region; (7) median line length: length of the line connecting the mid points of the lines between the corresponding dorsal and ventral points; (8) thickness: ratio of the area to the median line length of the region; and (9) slenderness: ratio of the median line length to the thickness of the region.

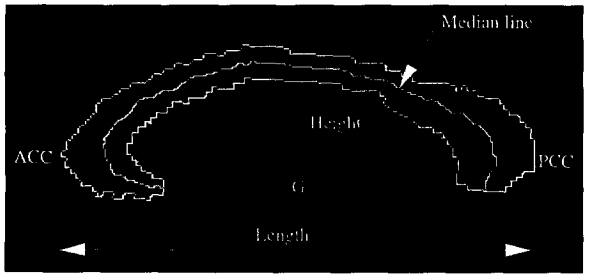

Fig. 3. Illustration of reference point G as the midpoint of ACC-PCC line. The median line is obtained by connecting the midpoints of corresponding points on the ventral and dorsal boundaries.

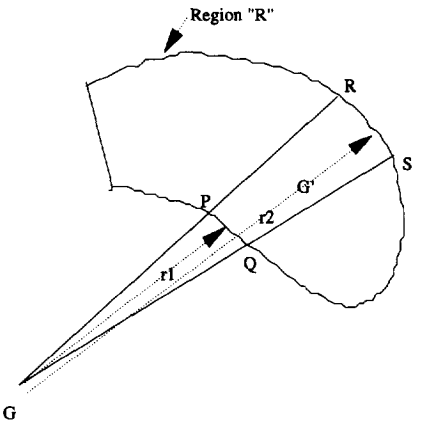

Fig. 4. Measurements of area and shape parameters of region **R** using smaller regional sectors ; PQSR denotes a representative sector in the region and r_1 and r_2 are the average distances from G to PQ and RS boundary segments, respectively.

The values of the above parameters were computed using the equations derived in the Appendix. In the derivations, it was assumed that the dorsal and ventral boundaries of the sectors were portions of arcs with fixed radii. This assumption is valid only if the lengths of the ventral and dorsal boundaries of the sectors are small, and the distances to the boundary points from the reference point do not deviate significantly within a sector. To achieve this, the CC was partitioned into a large number of sectors and the averages of the lengths to the boundary points from the reference point were used as distances to the ventral and dorsal boundaries. The smallest possible size of the sector is determined by the resolution of the images and limited by the pixel dimensions. In this report, we used $N = 100$ because it yielded acceptable results and was easy to compare the results with the work of others [54–56].

Parameters of the CC were computed using all the sectors. In addition to the above parameters, the length and height of the CC, defined to be the distances between the ACC and PCC points and between G and the dorsal boundary point directly above the reference point, respectively (see Fig. 3), were measured.

The shape program, which was written in C language, is available upon request.

3. RESULTS

3.1. Reliability

Because the measurement of parameters from the CC outline is fully automated, the reliability of the technique depends on the

Table 1 *Interrater and intrarater interclass correlation coefficients (ICC's) for parameters of the corpus callosum computed over 20 subjects*

Measurement	Intrarater reliability	Interrater reliability
Area	0.99	0.99
Perimeter	0.99	0.98
Compactness	0.96	0.98
Length	0.99	0.99
Width	0.95	0.88
Height	0.95	0.92
Median line length	0.98	0.96

process of selecting the midsagittal plane and extracting the CC outline thereof. The CC outlines of 20 subjects were obtained twice by the same operator, and the parameters of the CC were evaluated to determine the intrarater reliabilities. The same 20 subjects were used by another independent rater to extract the outlines to obtain the CC parameters to determine interrater reliabilities.

The intrarater and interrater interclass correlation coefficients (ICC's) [66] computed for the parameters of the CC are shown in the Table 1. Since the intrarater ICC's were high, all CC traces in our data base of 410 MRI brain scans were extracted by the same rater (A.C.V.), who was blind to the subject characteristics.

3.2. Comparison of area with pixel counts

With digitization of the images, the boundaries of the CC follow the edges of the quadratic pixels, and therefore, are not smooth curves. Due to their finite size, the pixels at the boundaries may contain other tissues in addition to those belong to the CC. Also some such pixels may not be included in the area of the CC. This introduces partial volume effects resulting in errors in area measurements based on pixel counting and in shape measurements based on boundary lengths. As seen in the Fig. 1, when the images are enlarged, this artifact is further intensified and the boundaries of the CC take a stepwise pattern.

The present method assumes that the CC is a natural structure having smooth boundaries and approximates the ventral and dorsal boundaries of the sectors with arcs in the derivation of area and shape parameters (Appendix). This partially accounts for partial volume effects at the boundaries and errors due to the digitization effects along boundary lengths. Area measures obtained by the present method were compared with those obtained by pixel counting in Table 2, and their correlations were high. In the rostrum, the smallest of the subdivisions, area measurements derived from pixel counting method were slightly larger than the area measurements derived using our method.

Table 2 *Comparison of corpus callosum area measurements with pixel counting technique based on measurements of 104 healthy children and adolescents*

Region (areas)	Correlation coefficients	RMS difference (%)
Rostrum	0.96	7.7
Genu	0.97	2.3
Rostral body	0.99	0.7
Anterior midbody	0.97	1.8
Posterior midbody	0.97	2.7
Isthmus	0.99	0.7
Splenium	0.99	1.1
Corpus callosum	0.99	0.1

The differences are given in root mean square (RMS) values.

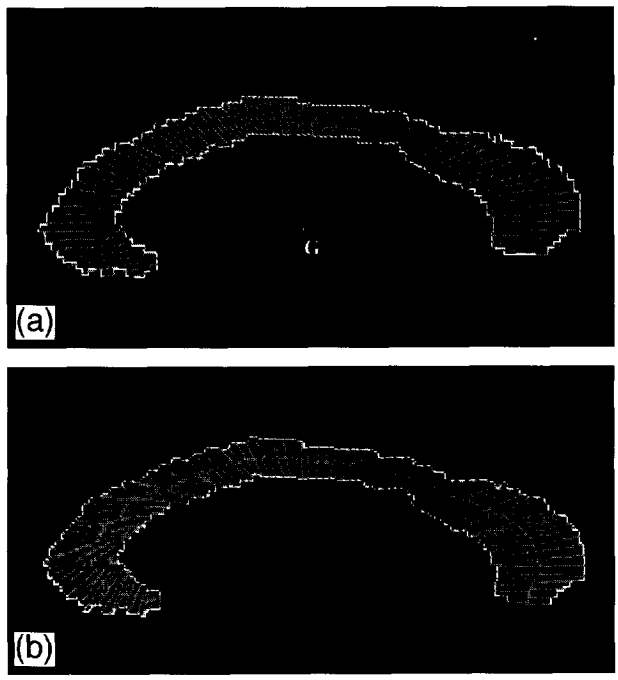

Fig. 5. a: 100 regional sectors obtained by equally dividing the angle subtended by the corpus callosum on the reference point G; b: regional sectors obtained by connecting 100 equally spaced points on ventral and dorsal boundaries.

3.3. Comparison with other methods using line segments

The present method utilizes the average distances to the dorsal and ventral boundaries of the sectors of the CC to compute regional size and shape parameters. Clarke et al. [24] used the same midline generated by these sectors but made use of line segments passing through 29 equally spaced points on the midline to derive a bulbosity index for the posterior regions of the CC. Denenberg et al. [16,55,56] subdivided the CC into 99 sectors using 100 line segments connecting equally spaced corresponding points on dorsal and ventral boundaries. To divide the CC boundaries into dorsal and ventral portions, the tips of the rostrum and splenium were selected so as to minimize the sum of the lengths of the line segments. The line segments were then clustered using factor analysis and parsed the CC into seven statistically different regions [55,56].

The line segments produced by radial lines through the center of gravities of the sectors generated by the present method and by the scheme adopted by Denenberg et al. [55,56] on a CC are shown in Fig. 5a and Fig. 5b, respectively. Averages of these lengths over our sample are plotted in Fig. 6 starting with line indexes from the tip of the rostrum. The lengths of line segments of the two schemes disagree at the most anterior and posterior portions of the CC. A major advantage of using line segments based on divisions of ventral and dorsal boundaries is the independence of the measurements to the orientation and curvature of

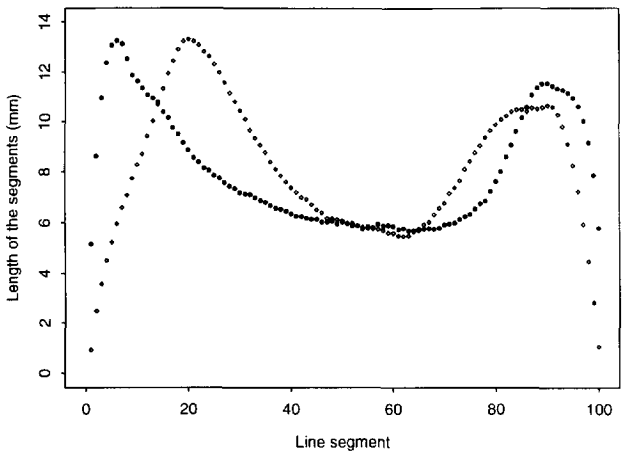

Fig. 6. Comparison of lengths of 100 line segments obtained by radial lines drawn from a reference point and by connecting equally spaced dorsal and ventral boundary points; ●, lines generated by radial lines from a reference point; ♦, lines connecting equally spaced dorsal and ventral boundary points. Average lengths were computed over the outlines of corpus callosa of 104 healthy children and adolescents.

the CC. However, due to the digitization effects and noise at the boundaries, the line segments generated using boundary points may not partition the median line uniformly and produce uniform sectors.

3.4. Pediatric MR images

Size and shape parameters of the CC's were acquired for 104 right-handed healthy children and adolescents (57 male and 47 female). The mean and standard deviation of parameters for the CC parameters are presented in Table 3. Area measurements of the subregions have been reported elsewhere [63].

Linear regression analyses were performed for the parameters in relation to age for males and females separately. The results for the CC and its subregions are shown in the Tables 4 and 5, respectively. Gender differences were analyzed using ANOVA and then ANCOVA with the total cerebral volume to adjust for the approximately 9% larger total cerebral volume in males [63].

As seen in Table 4, all of the CC parameters, except for slenderness and height for males, increased significantly ($P < 0.05$) with age in both sexes. Increased compactness indicates that the boundary of the CC becomes more regular and less complex with age. The CC elongates in the ACC-PCC direction from ages 4 to 18, while increases in thickness and width of the CC demonstrate its growth in lateral directions. ANOVA analyses indicated that the ACC-PCC length of the CC increased more rapidly in males than in females. But, when the length of the CC was adjusted for cerebral volume by ANCOVA analyses, this gender difference disappeared.

As reported in [48] and seen in the Table 5, areas of the posterior and midbody regions increased significantly ($P < 0.05$) in both males and females from ages 4 to 18. There was a trend for an increase in the rostral body area in males. The greatest enlargement of area was seen in the splenium with 5.93 mm^2/year for males and 4.72 mm^2/year increase for females. There were no gender differences in rates of increase in areas in any of the subregions of the CC.

Distances from the reference point to the center of gravities of the subregions, except at the midbody regions, increased significantly in both sexes indicating changes in the curvature of the midline at the anterior and posterior regions of the CC with age. The rates of changes of the distances to the anterior and posterior regions from the reference point were significantly different ($P < 0.05$) between males and females in an ANOVA analysis. However, this difference was not significant when corrected for cerebral volume in ANCOVA analysis.

Like the areas, the perimeter of the posterior regions and midbody regions significantly increased ($P \leq 0.001$) with age, except at the isthmus for males. The compactness of the splenium, isthmus and posterior midbody increased with age ($P < 0.05$) for both sexes, the anterior midbody increased in females ($P < 0.01$) and the rostral body increased in males ($P = 0.004$). There were no significant differences in rates of changes of the compactness in any of the regions between males and females.

Both the average width and maximum width were measured in all subregions. Maximum width measures 'bulbosity' of the region, whereas the average width measures 'wideness' lateral to the median line of the region. Both widths of the splenium and isthmus increased significantly in both sexes ($P < 0.05$) with respect to age. Further, in females, the maximum width increased significantly in the midbody and rostral body areas, but the rates of increase did not differ significantly between genders.

Table 3 *Means and standard deviations (S.D.) of the parameters for the corpus callosum measured over 57 male and 47 female children and adolescents from age 4 to 18*

Measurement	Male		Female	
	Mean	S.D.	Mean	S.D.
Area	613.99	83.69	600.34	70.14
Perimeter	146.94	13.06	143.69	15.19
Compactness	13.36	1.27	13.37	1.27
Length	71.28	5.22	69.27	4.60
Median line length	73.47	6.54	71.84	7.59
Width	7.78	0.72	7.78	0.84
Thickness	8.35	0.80	8.35	0.88
Height	17.62	2.47	16.92	2.32
Slenderness	8.87	1.12	8.69	1.27

The distances are in mm and the areas are in mm^2.

Table 4 *Regression analyses of the corpus callosum parameters of 104 (57 male and 47 female) healthy right-handed children and adolescents with age from 4 to 18 years*

Parameter	Regression analysis				ANOVA	
	Male		Female		Male vs. female	
	β-slope	*P*-value	β-slope	*P*-value	*P*-value	comment
Area	11.15	< 0.001	12.11	< 0.001	0.336	
Perimeter	1.11	0.028	1.52	0.006	0.214	
Compactness	0.15	0.003	0.13	0.009	0.884	
Length	0.85	< 0.001	0.49	0.003	0.029	male > female
Median line length	0.56	0.028	0.76	0.006	0.214	
Width	0.07	0.014	0.09	0.006	0.888	
Thickness	0.09	0.003	0.08	0.009	0.884	
Height	0.14	0.149	0.25	0.003	0.111	
Slenderness	0.03	0.490	0.01	0.913	0.473	

ANOVA analyses compare the slopes of changes with age between males and females.

Except for the isthmus in females, median line lengths of the regions significantly increased in the posterior and midbody regions in both sexes ($P < 0.001$). Thickness, which gives an average width measure less sensitive to random variation of the boundaries, significantly increased in posterior regions in both sexes and in midbody regions only in females. Slenderness did not significantly change with age in any of the subregions. Median line length, thickness and slenderness did not show sexual dimorphism in any of the CC subregions.

4. DISCUSSION

The automated method presented here computes size and shape parameters of the CC and its subregions from its tracing on the midsagittal plane. The method improves on previous methods which give only the midsagittal areas of the CC and its subregions, and provides sensitive and reliable measurements to identify subtle shape variations of the CC in the developing brain. The main advantage of the method is that the computation of summations of distances to the ventral and dorsal boundaries of a large number of regional sectors from a reference point produces a multitude of parameters representing the complex shape of the CC and its subregions. Other advantages include simplicity in implementation, speed which allows application to a large data set, and the absence of user-specific errors. Once the CC trace is extracted from the midsagittal plane in a supervised manner, the program automatically finds the regional divisions and associated parameters of the CC. Since the method approximates a smooth boundary along the periphery of the CC, the digitization and partial volume effects are minimized in computation of the parameters unlike pixel counting technique which follows stepwise boundaries along the pixel edges.

The selection of the ACC and PCC points was crucial to our method since the subsequent measurements were taken in reference to the midpoint of ACC-PCC line and the regional subdivisions were based on ACC-PCC length. Moreover, the divisional lines were vertically drawn from ACC-PCC line making standardization of the orientation, often neglected in previous studies [10], of great importance. The present method iteratively oriented the ACC-PCC line while verifying for the locations of the ACC and PCC points. Witelson's scheme of subdivisions of the CC assumes that the functionally different cortical regions span from anterior to posterior directions in the hemispheres. The sulcal and gyral patterns which demarcate the cortical regions are not exactly vertical and sometimes almost horizontal (e.g., temporal regions). Some researchers prefer radial dividing lines or divisions based on the median line of the CC with the presumption that the fiber tracts span radially to the cortical region. Although the present technique quantifies the subdivisions proposed by Witelson [10], it can easily be extended to other schemes of subdivisions since the sectors are based on radial lines and the midline can be derived conveniently.

Comparison of our results with the pixel counting technique revealed similar area estimates except for the rostrum. Our technique may not be accurate in quantifying the rostrum since it is relatively a small region and only a few sectors comprise the whole rostrum. A large number of sectors may increase the accuracy of the measurement, but may result in instability of computations due to the digitization and noise effects at the boundaries. One hundred sectors produced acceptable results with our technique and was also the choice of Denenberg et al. [54–56].

The size and shape of the CC depend on the number and the size of callosal fibers and their packing density and myelination patterns. Major changes of the CC take place approximately 2–3 months postnatally when the number of fibers across the CC becomes maximal [67]. Subsequent morphological changes are subtle and less regular and may not be due to the generation of new fibers. Although Yakovlev and Lecours [68] indicated that CC myelination levels reached the adult values by age 10, more recent studies [12,15,44,45] show the callosal area to increase up to the third decade of life. The present study signifies important size and shape variations also taking place between ages 4 to 18, mostly in splenium and isthmus of the CC, as our previous study [48] found that the anterior regions had reached adult values by age 5.

The median line length was preferred by some researches over the ACC-PCC length to express the length of CC as the median line compensates for the curling at genu and splenium. Although there was no significant gender difference between the rates of increase of the median line length, ACC-PCC line length in males increased at a higher rate than that in females with age. This difference of the CC growth in gender has not been previ-

Table 5 *Regression analyses of regional parameters of the corpus callosa of 104 (57 male and 47 female) healthy right-handed children and adolescents with ages 4 to 18. ANOVA analyses compare the rates of changes of the parameters with age between male and female populations*

Region	Parameters	Male		Female		ANOVA	
		β-slope	*P*-value	β-slope	*P*-value	*P*-value	Comment
Splenium	area	5.93	< 0.00	4.72	< 0.001	0.276	male > female
	perimeter	0.73	< 0.001	0.68	< 0.001	0.516	
	compactness	0.24	< 0.001	0.16	< 0.001	0.362	
	distance to CG	0.36	< 0.001	0.19	0.004	0.014	
	width	0.18	< 0.001	0.12	< 0.001	0.427	
	maximum width	0.28	< 0.001	0.14	0.005	0.908	
	median line length	0.30	< 0.001	0.29	0.001	0.405	
	thickness	0.18	< 0.001	0.12	< 0.001	0.445	
	slenderness	−0.01	0.502	0.00	0.833	0.789	
Isthmus	area	1.32	0.004	1.50	< 0.001	0.605	male > female
	perimeter	0.28	0.138	0.64	< 0.001	0.770	
	compactness	0.08	< 0.001	0.06	0.004	0.485	
	distance to CG	0.17	0.006	0.15	0.017	0.015	
	width	0.09	< 0.001	0.06	0.010	0.805	
	maximum width	0.19	0.003	0.10	0.045	0.938	
	median line length	0.06	0.303	0.20	< 0.001	0.485	
	thickness	0.09	< 0.001	0.06	0.011	0.774	
	slenderness	−0.05	0.032	0.01	0.775	0.645	
Posterior midbody	area	1.23	0.004	1.65	< 0.001	0.934	male > female
	perimeter	0.40	0.001	0.58	< 0.001	0.560	
	compactness	0.05	0.056	0.06	0.029	0.555	
	distance to CG	0.10	0.268	0.06	0.016	0.078	
	width	0.03	0.282	0.06	0.016	0.679	
	maximum width	0.05	0.219	0.08	0.017	0.866	
	median line length	0.17	< 0.001	0.16	< 0.001	0.453	
	thickness	0.03	0.282	0.07	0.011	0.642	
	slenderness	0.01	0.469	0.00	0.797	0.345	
Anterior midbody	area	1.04	0.013	1.54	< 0.001	0.238	male > female
	perimeter	0.39	0.001	0.51	< 0.001	0.328	
	compactness	0.03	0.144	0.05	0.010	0.235	
	distance to CG	0.12	0.149	0.14	0.065	0.034	
	width	0.01	0.563	0.06	0.016	0.371	
	maximum width	0.01	0.891	0.06	0.070	0.777	
	median line length	0.17	< 0.001	0.15	< 0.001	0.229	
	thickness	0.01	0.594	0.06	0.013	0.378	
	slenderness	0.03	0.039	0.00	0.946	0.845	
Rostral body	area	1.17	0.073	1.00	0.144	0.787	male > female
	perimeter	−0.01	0.959	0.33	0.172	0.413	
	compactness	0.07	0.004	0.03	0.290	0.777	
	distance to CG	0.23	0.003	0.15	0.049	0.020	
	width	0.05	0.033	0.03	0.298	0.513	
	maximum width	0.04	0.033	0.11	0.393	0.305	
	median line length	0.05	0.620	0.12	0.201	0.281	
	thickness	0.05	0.029	0.02	0.330	0.511	
	slenderness	−0.04	0.176	0.00	0.853	0.216	
Genu	area	−0.37	0.730	0.97	0.377	0.407	
	perimeter	−0.40	0.128	0.22	0.454	0.888	
	compactness	0.04	0.494	0.04	0.403	0.260	
	distance to CG	0.37	< 0.001	0.22	0.010	0.117	
	width	0.03	0.496	0.04	0.370	0.298	
	maximum width	0.06	0.333	0.05	0.355	0.071	
	median line length	−0.14	0.106	0.07	0.461	0.961	
	thickness	0.07	0.444	0.04	0.374	0.267	
	slenderness	−0.03	0.198	0.00	0.893	0.406	
Rostrum	area	0.81	0.083	0.72	0.160	0.808	
	perimeter	0.10	0.597	0.21	0.355	0.530	
	compactness	0.12	0.013	0.62	0.184	0.420	
	distance to CG	0.29	< 0.001	0.15	0.033	0.480	
	width	0.11	0.122	0.06	0.218	0.354	
	maximum width	0.18	0.036	0.10	0.192	0.707	
	median line length	0.05	0.485	0.08	0.303	0.481	
	thickness	0.11	0.051	0.05	0.221	0.384	
	slenderness	−0.03	0.150	−0.01	0.836	0.170	

ously reported in the literature. However, the sex differences in growth of the CC length disappeared after adjustment for cerebral volumes.

The perimeter supplements the area measurements while the compactness and slenderness render the 'form' and 'complexity' of the boundaries of the region relative to their size. Our results indicate that the CC boundaries become more regular and less complex from age 4 to 18, particularly at the midbody and posterior regions. Since the brain size is unchanged during this age span [48], these shape variations do not depend on the brain size. As it acquires more matured adult configuration, CC shape may configure into a more regular and compact form. The curvature of the CC, measured by the distances to the subregions from the reference point, increased with age in the anterior and posterior regions of the CC for the both sexes, with a higher rate of increase with age in males. However, this gender effect in the curvature growth is not preserved after adjustment for cerebral size.

The width and thickness furnish information about the average size of a region lateral to the median line. The lateral growth was also restricted to the posterior regions of the CC. The maximum width, measured as the maximum radial length between ventral and dorsal boundaries, gives an idea of 'bulbosity' of the region. There was no sex differences in the maximum width of the splenium in contrast to the reported sexual dimorphism in the bulbosity of the splenium [19,20] for an adult sample. This may be due to the differences between the bulbosity indexes used by others and the maximum width measure used in this study, or the average age of subjects used in the studies.

In adults, sexual dimorphism in total CC area, splenium area and bulbosity has been reported [18–20,22–28,24], although not universally [10,14,17,21,69]. We failed to find sex differences for our sample of children and adolescents after controlling for brain size as recommended by others [70]. This suggests that the gender differences in the CC reported elsewhere may be related to the differences in the brain sizes between genders [45,63]. For our 104 pediatric subjects, we found significant correlations ($r > 0.3$ and $P < 0.001$) between the CC area and the areas of the genu, midbody, and splenium with the cerebral volume.

In summary, the method presented here can be applied reliably and accurately to determine the size and shape of the CC and its subregions. The method was used to demonstrate the different growth patterns and characteristics of shapes of different CC regions from age 4 to 18 using a large sample. Although the subjects used here were of ages beyond 4 years. the major changes of myelination takes place before this age span and the present method may be useful in the analysis of the CC of infants and neonates. The type of shape parameters used here may become valuable when measuring callosa of clinical populations whose brain morphology has been distorted due to various pathological conditions. The method will be used to compare the size and shape measurements of the CC of patients with childhood onset neuropsychiatric disorders.

Appendix A. Measurement of size and shape parameters

Consider the region **R** and the sector PQSR shown in Fig. 4. Let θ be the angle subtended by the sector on the reference point G, and G′ be the center of the gravity of the sector PQSR. r_1 and r_2 are the average lengths from G to boundary curves PQ and SR. The length GG′ is given by:

$$GG' = \frac{r_1 + r_2}{2}$$

Assuming that PQ and SR are arcs from circles, the lengths PQ and RS:

$$PQ = r_1 \cdot \theta \text{ and } SR = r_2 \cdot \theta$$

With the same assumption, the areas GPQ, GRS, and PQSR are given by:

$$GRP = \frac{1}{2} r_1^2 \cdot \theta \text{ and } GRS = \frac{1}{2} r_2^2 \cdot \theta$$

$$PQSR = GRS - GPQ = \frac{1}{2}(r_2 - r_1)(r_2 + r_1)$$

For the region **R**, the parameters are calculated by averaging or summing the parameters over all the segments that comprise the region. If N is the number of sectors in region **R**:

$$area = \sum_R PQSR = \sum_R \frac{1}{2}(r_2 + r_1) \cdot (r_2 - r_1) \cdot \theta = \frac{1}{2}\theta \cdot S_3$$

$$perimeter = \sum_R (PQ + SR) = \sum_R (r_1 + r_2) \cdot \theta = \theta \cdot (S_1 + S_2)$$

$$median\ line\ length = \sum_R \frac{PQ + SR}{2}$$

$$= \frac{1}{2}\sum_R (r_1 \cdot \theta + r_2 \cdot \theta) = \frac{1}{2} \cdot \theta \cdot (S_1 + S_2)$$

$$distance\ to\ CG = \text{ave}\left\{\frac{r_1 + r_2}{2}\right\} = \sum_R \frac{r_1 + r_2}{2N} = \frac{1}{2N} \cdot (S_1 + S_2)$$

$$maximum\ width = \max\{r_2 - r_1\}$$

The other parameters can be evaluated using the above results and their definitions:

$$compactness = \frac{area}{perimeter}$$

$$thickness = \frac{area}{median\ line\ length}$$

$$slenderness = \frac{median\ line\ length}{thickness}$$

REFERENCES

1. Tomasch J. Size, distribution, and number of fibers in the human corpus callosum. *Anat Res* 1954; **119**: 119–35.
2. Demeter S, Ringo JL, Doty RW. Morphometric analysis of the human corpus callosum and anterior commissure. *Hum Neurobiol* 1988; **6**: 219–26.
3. De Lacoste MC, Kirkpatrick JB, Ross ED. Topography of human corpus callosum. *J Neuropathol Exp Neurol* 1985; **44**: 578–91.
4. Pandya DN, Seltzer B. The topography of commissural fibers. In: Lepoie F, Ptito M, Jaspar H, eds. *Two hemispheres — one brain: Functions of the corpus callosum*. New York: Alan Liss, 1986; 47–73.

5. Bogen JE. Split-brain Syndromes. In: Vinken PJ, Bruyn, Klawans HL, Fredericks JAM, eds. *Handbook of clinical neurology, vol 45. Revised series 1. Clinical neuropsychology.* Amsterdam: Elsevier, 1985: 99–106.
6. Zaidel E, Clarke JM, Suyenobu B. Hemispheric independence: a paradigm case for cognitive neuroscience. In: Scheibel A, Wechsler A, eds. *Neurobiology of higher order cognitive function.* New York: The Guilford Press, 1990: 297–355.
7. Myers RE, Sperry RW. Interhemispheric communication through the corpus callosum. *A M A Arch Neurol Psychiatry* 1958; **80**: 298–303.
8. Sperry RW, Gazzaniga MS, Bogen JE. Interhemispheric relationships: The neocortical commissures; syndromes of hemisphere disconnection. In: Vinken PJ, Bruyn GW, eds. *Handbook of clinical neurology, vol 4, Disorders of speech, perception, and symbolic behaviour*, Amsterdam: Elsevier, 1969: 273–90.
9. Witelson SF. The brain connection: the corpus callosum is larger in left-handers. *Science* 1985; **229**: 665–8.
10. Witelson SF. Hand and sex differences in the isthmus and genu of the human corpus callosum. *Brain* 1989; **112**: 799–835.
11. Witelson SF, Kigar DL. Anatomical development of corpus callosum in humans: A review with reference to sex and cognition. In: Molefese DL, Segalowitz SJ, eds. *Brain lateralization in children: Development implications.* New York: The Guilford Press, 1988: 35–7.
12. Allen LS, Richey MF, Chai YM, Gorski RA. Sex differences in the corpus callosum of the living human being. *J Neurosci* 1991; **11**: 933–42.
13. Kertesz A, Polk M, Howell J, Black SE. Cerebral dominance, sex, and callosal size in MRI. *Neurology* 1987; **37**: 1385–8.
14. Bell AD, Variend S. Failure to demonstrate sexual dimorphism of the corpus callosum in childhood. *J Anat* 1985; **143**: 143–7.
15. Cowell PE, Allen LS, Zalatimo NS, Denenberg VH. A development study of sex and age interactions in the human corpus callosum. *Dev Brain Res* 1992; **66**: 187–92.
16. Berrebi AS, Fitch RH, Ralphe DL, Denenberg JO, Friedrich VL, Denenberg VH. Corpus callosum: region-specific effects of sex, early experience and age. *Brain Res* 1988; **438**: 216–24.
17. Byne W, Bleier R, Houston L. Variations in human corpus callosum do not predict gender: a study using magnetic resonance imaging. *Behav Neurosci* 1988; **102**: 222–7.
18. De Lacoste-Utamsing C, Holloway RL. Sexual dimorphism in the human corpus callosum. *Science* 1982; **216**: 1431–2.
19. De Lacoste M-C, Holloway RL, Woodward DJ. Sex differences in the fetal human corpus callosum. *Hum Neurobiol* 1986; **5**: 93–6.
20. Holloway RL, de Lacoste MC. Sexual dimorphism in the human corpus callosum: an extension and replication study. *Hum Neurobiol* 1986; **5**: 87–91.
21. Oppenheim JS, Lee BCP, Nass R, Gazzaniga MS. No sex-related differences in human corpus callosum based on magnetic resonance imagery. *Ann Neurol* 1987; **21**: 604–6.
22. Potter SM, Graves RE. Is interhemispheric transfer related to handedness and gender. *Neuropsychologia* 1988; **26**: 319–25.
23. Habib M, Gayraud D, Oliva A, Regis J, Salamon G, Khalil R. Effects of handedness and sex on the morphology of the corpus callosum: a study with brain magnetic resonance imaging. *Brain Cogn* 1991; **16**: 41–61.
24. Clarke S, Kraftsik R, Van der loos H, Innocenti GM. Forms and measures of adult and developing human corpus callosum: is there sexual dimorphism? *J Comp Neurol* 1989; **280**: 213–30.
25. Raine A, Harrison GN, Reynolds GP, Sheard C, Cooper JE, Medley I. Structural and functional characteristics of the corpus callosum in schizophrenics, psychiatric controls and normal controls. *Arch Gen Psychiatry* 1990; **47**: 1060–4.
26. Swayze II VW, Andreasen NC, Ehrhardt JC, Yuh WTC, Alliger RJ, Cohen GA. Developmental abnormalities of corpus callosum in schizophrenia. *Arch Neurol* 1990; **47**: 805–8.
27. Woodruff PWR, Pearlson GD, Geer MJ, Barta PE, Chilcoat HD. A computerized magnetic resonance imaging study of corpus callosum morphology in schizophrenia. *Psychol Med* 1993; **23**: 45–56.
28. Gabrielle O, Salvolini U, Bonifazi V, et al. Morphological studies of the corpus callosum by MRI in children with malformative syndromes. *Neuroradiology* 1993; **35**: 109–12.
29. Nasrallah HA, Andreasen NC, Coffman JA, et al. A controlled magnetic resonance imaging study of corpus callosum thickness in schizophrenia. *Biol Psychiatry* 1986; **21**: 274–82.
30. Hynd GW, Semrud-Clikeman M, Lorys AR, Novey ES, Eliopulos D, Lyytinen H. Corpus callosum morphology in attention deficit-hyperactivity disorder: morphometric analysis of MRI. *J Learn Disab* 1991; **24**: 141–6.
31. Schaefer GB, Bodensteiner JB, Thompson JN, Wilson DA. Clinical and morphometric analysis of the hypoplastic corpus callosum. *Arch Neurology* 1991; **48**: 933–6.
32. Laissy JP, Patrux B, Duchateau C, et al. Midsagittal MR measurements of the corpus callosum in healthy subjects and diseased patients: A prospective survey. *AJNR* 1993; **14**: 145–54.
33. Giedd JN, Castellanos FX, Casey BJ, et al. Quantitative morphology of the corpus callosum in attention deficit hyperactivity disorder. *Am J Psychiatry* 1994; **151**: 665–9.
34. Hoff AL, Neal C, Kushner M, DeLisi LE. Gender differences in corpus callosum size in first-episode schizophrenics. *Biol Psychiatry* 1994; **35**: 913–9.
35. Scott TF, Price TRP, George MS, Brillman J, Rothfus W. Midline cerebral malformations and schizophrenia. *J Neuropsychiatry* 1993; **5**: 287–93.
36. Raffel C, Kongelbeck SR, Snead IIIOC. Corpus callosotomy for intractable epilepsy in children. *Pediatr Neurosurg* 1992; **18**: 305–9.
37. Semrud-Clikeman M, Filipek, PA, et al. Attention-deficit hyperactivity disorder: magnetic resonance imaging morphometric analysis of the corpus callosum. *J Am Acad Child Adolesc Psychiatry* 1994; **33**: 875–81.
38. David AS. Callosal transfer in schizophrenia: too much or too little? *J Abnorm Psychol* 1993; **102**: 573–9.
39. David A. Schizophrenia and the corpus callosum: developmental, structural and functional relationships. *Behav Brain Res* 1994; **64**: 203–11.
40. Pelletier J, Habib M, Lyon-Caen O, Salamon G, Poncet M, Khalil R. Functional and magnetic resonance imaging correlates of callosal involvement in multiple sclerosis. *Arch Neurol* 1993; **50**: 1077–82.
41. Colombo C, Bonfanti A, Scarone S. Anatomical characteristics of the corpus callosum and clinical correlates in schizophrenia. *Eur Arch Psychiatry Clin Neurosci* 1994; **243**: 244–8.
42. Wang ZP, Osawa M, Fukuyama Y. Morphometric study of the corpus callosum in Fukuyama type congenital muscular dystrophy by magnetic resonance imaging. *Brain Dev* 1995; **17**: 104–10.
43. Rakic P, Yakovlev PI. Development of the corpus callosum, and cavum septi in man. *J Comp. Neurol* 1978; **132**: 45–72.
44. Pujol J, Vendrell P, Junque C, Marti-Vilalta JL, Capdevila A. When does human brain development end? evidence of corpus callosum growth up to adulthood. *Ann Neurol* 1993; **34**: 71–5.
45. Rauch RA, Jinkins JR, Analysis of cross-sectional area measurements of the corpus callosum adjusted for brain size in male and female subjects from childhood and adulthood. *Behav Brain Res* 1994; **64**: 65–78.
46. Rowe LA, Kranzier J, Lombardino LJ, et al. Corpus callosum development in children. *Abstract presented at the 24th annual meeting of the Society for Neuroscience,* Miami, FL, 1994; 20.
47. Barkovich AJ, Kjos BO. Normal postnatal development of the corpus callosum as demonstrated by MR imaging. *AJNR* 1988; **9**: 487–91.
48. Giedd JN, Rumsey JM, Castellanos FX, et al. A quantitative MRI study of the corpus callosum in children and adolescents. *Dev Brain Res*, 1996; **91**: 274–80.
49. Cowell PE, Kertesz A, Denenberg VH. Multiple dimensions of handedness and the human corpus callosum. *Neurology* 1993; **43**: 2353–7.

50. Steinmetz H, Jancke L, Kleinschmidt A, Schlaug G, Volkmann J, Huang Y. Sex but no hand difference in the isthmus of the corpus callosum. *Neurology* 1992; **42**: 749–52.
51. O'Kusky J, Strauss E, Kosaka B, et al. The corpus callosum is larger with right-hemisphere cerebral speech dominance. *Ann Neurol* 1988; **24**: 379–83.
52. Hines M, Chiu L, McAdams LA, Bentler PM. Cognition and the corpus callosum: Verbal fluency, visuospatial ability and language lateralization related to midsagittal surface areas of callosal subregions. *Behav Neurosci*, 1992; **106**: 3–14.
53. Reinarz SJ, Coffman CE, Smoker WRK, Godersky JC. MR imaging of corpus callosum: Normal and pathologic findings and correlation with CT. *AJNR* 1988; **9**: 649–56.
54. Denenberg VH, Berrebi AS, Fitch RH. A factor analysis of the rat's corpus callosum. *Brain Res* 1989; **497**: 271–9.
55. Denenberg VH, Kertesz A, Cowell PE. A factor analysis of the human's corpus callosum. *Brain Res* 1991; **548**: 126–32.
56. Denenberg VH, Cowell PA, Fitch RH, Kertesz A, Kenner GH. Corpus callosum: multiple parameter measurements in rodents and humans. *Psychol Behav* 1991; **49**: 433–7.
57. Bracewell RN. The Fourier transform. *Sci Am* 1989; 260: 62–9.
58. Zahn CT, Roskies RZ. Fourier descriptors for plane closed curves. *IEEE Trans on Computers* 1972; **C-21**: 269–81.
59. Persoon E, Fu K. Shape discrimination using Fourier descriptors. *IEEE Trans Systems, Man and Cybernetics* 1977; **SMC-7**: 170–9.
60. He Y, Kundu A. 2-D shape classification using hidden Markov mode. *IEEE Trans on Pattern Analysis and Machine Intelligence* 1991; **13**: 1172–84.
61. Jain AK. *Fundamentals of digital image processing*. NJ, Prentice Hall: 1989.
62. Casanova MF, Sanders RD, Goldberg TE, et al. Morphometry of the corpus callosum in monozygotic twins discordant for schizophrenia: a magnetic resonance study. *J Neurol* 1990; **53**: 416–21.
63. Geidd JN, Snell JW, Lange N, et al. Quantitative magnetic resonance imaging of human brain development: ages 4–18. *Cerebral Cortex*, In press.
64. Denckla MB. Revised physical and neurological examination for subtle signs. *Psychopharmacology Bulletin* 1985; **21**: 773–800.
65. Rasband W. *NIH image manual*, Bethesda, MD: National Institutes of Health, 1993.
66. Bartko JJ, Carpenter WT. On the methods and theory of reliability. *J Nerv Ment Dis* 1976; **16**: 307–17.
67. Huttenlocher PR, De Courten C, Garey LJ, Van der Loos H. Synaptogenesis in human visual cortex: Evidence for synaptic elimination during normal development. *Neurosci Lett* 1982; **33**: 247–52.
68. Yakovlev PI, Lecours AR. The myelogenetic cylces of regional maturation of the brain. In Minkowske A, ed. *Regional development of the brain in early life*. Oxford: Blackwell Scientific, 1967: 3–70.
69. Weis S, Weber G, Wenger E, Kimbacher M. The controversy about sexual dimorphism of the corpus callosum. *Int J Neurosc*. 1989; **47**: 167–73.
70. Holloway RL, Anderson PJ, Defendini R, Harper C. Sexual dimorphism of the human corpus callosum from three independent samples: relative size of the corpus callosum. *Am J Phys Anthropol* 1993; **92**: 481–98.